Evaluation of Electromagnetic Coupling between Microelectronic Device Structures using Computational Electrodynamics

Wim Schoenmaker, Peter Meuris, Walter Pflanzl, and Alexander Steinmair

Abstract Electromagnetic coupling between devices in an microelectronic layout can become a serious design concern. In this paper, the problem of electromagnetic coupling is addressed from field computational point of view. Approximation schemes are justified by evaluating dimensionless parameters in the set up of the field equations and scale considerations of devices. The discretization scheme is reviewed and a simulation method is presented to compute the S-matrix directly by imposing boundary conditions that map directly to the experimental set up. An example demonstrates the validity of the scheme.

1 Introduction

With the use of increasing frequency ranges, electromagnetic coupling becomes a more pronounced design concern because induced electric fields are proportional to the rate of change of the magnetic induction. However, not only the pace of time variations are determining for including electromagnetic coupling but also the problem scale and the intensity of the currents that are responsible for the induced fields must be considered. An overall picture of the scaling arguments is presented in Section 2 which helps to identify the needed steps and inclusion of non-negligible effects. Once we note from scale considerations that electromagnetic coupling terms represent a non-negligible contribution to the full system of equations, we move to the the solution of these equations. In section 3, we review and update the approach

Wim Schoenmaker, Peter Meuris
MAGWEL NV, Martelarenplein 13, B-3000 Leuven BELGIUM e-mail: wim.schoenmaker@magwel.com, peter.meuris@magwel.com

Walter Pflanzl, Alexander Steinmair
austriamicrosystems AG, Schloss Premstätten, A-8141 Unterpremstätten AUSTRIA e-mail: Walter.Pflanzl@austriamicrosystems.com, Alexander.Steinmair@austriamicrosystems.com

that was proposed some years ago by the first author and co-workers [1–3]. We will refer to this approach as 'computational electrodynamics'.

At several occasions we were inquired if this method is equivalent to the method based on Nedelec's edge elements [4,5]. The main difference is that we do not refer to test functions at all. Our method is more related to finite-integration techniques (FIT) [6,7].

Scale considerations are not the only an issue for deciding if some terms in the full system of Maxwell equations and constitutive laws can be neglected. When discussing the coupling of devices, it is also important to realize that different devices can have intrinsic or geometrical scales that differ orders of magnitude. In such scenarios the coupled problem is most easily split in computational domains. Computational electrodynamics gives, rather straightforwardly, a series of prescriptions for matching the interface conditions of the various domains.

Electromagnetic coupling of microelectronic devices is an RF issue and is most conveniently measured using s-parameters. In section 5, we present our method to compute these matrix elements. In fact, s-parameter extraction is straightforwardly achieved as a post-processing of the results of a computational electrodynamics problem with the appropriate setting of the boundary conditions.

In Section 6 we will present an example of a coupled problem, that we have addressed recently.

2 Scaling Rules for the Maxwell Equations

The use of scaling arguments is definitely not new to the field of computing in electromagnetic modeling. Well-known approximations are the so-called EQS (electro-quasi-static) and MQS (magneto- quasi-static) approximations. Approximations can be put in a different perspective by considering the scaling step that is necessary when converting the full set of equations to dimensionless equations before the actual computing can start. For our present argument it suffices to consider insulators and metals only. Diffusive currents in semiconductors can easily be added to the equations. Therefore, we start from the Maxwell equations in which $\mathbf{J}_c$ is the conductive current :

$$\mathbf{J}_c = \sigma\mathbf{E}\,, \qquad \mathbf{D} = \varepsilon_0\varepsilon_r\mathbf{E}\,, \qquad \mathbf{H} = \frac{1}{\mu_0\mu_r}\mathbf{B}\,, \tag{1}$$

$$\mathbf{E} = -\nabla V - \frac{\partial \mathbf{A}}{\partial t}\,, \qquad \mathbf{B} = \nabla\times\mathbf{A}\,. \tag{2}$$

We consider the Maxwell equations in the potential formulation. The Poisson equation is used to solve the scalar field in insulators and semiconducting regions and the current-continuity equation is used in metals to find the scalar potential. The electric system is :

$$\nabla.\left[\varepsilon\left(\nabla V + \mathrm{i}\omega\mathbf{A}\right)\right] + \rho = 0\,, \qquad \nabla.\left[\left(\sigma + \mathrm{i}\omega\varepsilon\right)\left(\nabla V + \mathrm{i}\omega\mathbf{A}\right)\right] = 0\,. \tag{3}$$

The Maxwell-Ampere equation is :

$$\nabla \times \left(\frac{1}{\mu}\nabla \times \mathbf{A}\right) - (\sigma + \mathrm{i}\omega\varepsilon)(-\nabla V - \mathrm{i}\omega\mathbf{A}) = 0\,. \tag{4}$$

This system must be completed with a gauge condition

$$\nabla \cdot \mathbf{A} + \mathrm{i}\omega\xi\varepsilon\mu V = 0\,, \tag{5}$$

where ξ is a parameter that allows us to slide over different gauge conditions. Now let L be the 'natural' length scale of the problem that is considered. For example $L = 1\mu$m. Furthermore, let T be the natural time scale, for example $T = 10^{-9}$ sec. It is possible to reformulate the equations (3) and (4) in *dimensionless* variables V and $\mathbf{A}$ and the set of equations is controlled by two dimensionless variables, K and ν

$$\nabla.\left[\varepsilon_r(\nabla V + \mathrm{i}\omega\mathbf{A})\right] + \rho = 0\,, \qquad \nabla.\left[(\sigma + \mathrm{i}\omega\varepsilon_r)(\nabla V + \mathrm{i}\omega\mathbf{A})\right] = 0\,, \tag{6}$$

and

$$\nabla \times \left(\frac{1}{\mu_r}\nabla \times \mathbf{A}\right) - K\omega^2(\varepsilon_r - \mathrm{i}\,\nu)\mathbf{A} - \mathrm{i}\,\omega K(\varepsilon_r - \mathrm{i}\nu)\nabla V = 0\,. \tag{7}$$

The constants $K = \varepsilon_0\mu_0 L^2/T^2$ and $\nu = \sigma T/\varepsilon_0$. Note that for $\sigma = 10^4$ S/m we obtain $K\nu = 10^{-5}$. This value corresponds to the conductance of an inversion layer in the on-state of a transistor. This number enters into the Maxwell-Ampere equation and suggests that in this scenario the magnetic sector is negligible. For a single transistor finger this is a valid conclusion, but one should be aware that in actual designs many fingers may operate in a parallel mode therefore the value of K could increase since L must be adapted to this situation. Taking into account the presence of the back-end processing, one encounters metallic conductance of 10^7 S/m, such that magnetic effects are important.

3 Discretization

In our earlier work, we presented a discretization method that decided for each variable where on the grid it belongs. It was concluded that the geometrical and physical meaning of variables plays a key role. For instance, a scalar variable, e.g. the Poisson potential, V, is a number assigned to each space location and for a computational purpose, its discretized value should be assigned to the nodes of the grid. On the other hand the vector potential $\mathbf{A}$ is a variable of the same character as ∇V and should therefore be assigned to the links of the computational grid. Geometrical considerations have been an important guide for correctly discretizing Maxwell's equations, as was also elaborated by Bossovit [8, 9].

The conversion of continuous variables to discrete variables on the computation grid also has consequences for the particular discretization route that is followed

when implementing discrete versions of the Maxwell equations. Gauss' law is discretized by considering elementary volumes around the nodes of the grid and one next perform an integration of Gauss' law over these volume cells. The flux assigned to each segment of the enclosing surface is assumed to be constant which allows for expressing this (constant) flux in terms of the node variables and link variables. This scheme has been the key to the success of the simulation of the semiconductor devices. The Scharfetter-Gummel formulation of the discretized currents can be set up following the above approach [10]. Since links variables are fundamentally different from node variables, we expect that the discretization of the Maxwell-Ampere equation has to be done taking this geometrical aspect into account. Whereas it was quite 'natural' to regard node variables as a representative of some volume element, in the same way we consider a link variable representing some area element. Thus to each link is associated an area element and in order to discretize the Maxwell-Ampere equation on a grid we now apply Stokes' law to arrive at the discretized equations.

After having obtained a scheme to discretize the Maxwell equations, we proceed with expanding them into a small signal analysis. This means that each variable is written as a time-independent part and an harmonic part

$$X = X_0 + X_1 \mathrm{e}^{\mathrm{i}\omega t} \ . \tag{8}$$

If we apply boundary conditions of a similar form and collect terms independent of ω and terms proportional to $\mathrm{e}^{\mathrm{i}\omega t}$ and omit terms proportional to X_1^2 then we obtain a system of equations for the phasors X_1. Of particular interest is the treatment of the spurious modes in the fields. These modes can be eliminated by selecting a 'gauge tree' in the mesh, adding a ghost field to the equation system or apply a projection method while iterating towards the solution. We can also apply a gauge condition and construct discrete operators that resemble the continuous operators as close as possible including having a semi-definite spectrum. Using a two-fold application of Stokes' law, the term $\nabla \times \left(\frac{1}{\mu_r} \nabla \times \mathbf{A} \right)$ appears in the discretized formulation as a collection of closed-loop circulations. By subtracting a discretized version of $\nabla (\nabla \cdot \mathbf{A})$ we arrive at an operator that resembles $-\nabla^2 \mathbf{A}$. However, since $\mathbf{A}$ is a vector field, the latter can only have meaning in terms of the foregoing expressions. The discretization of the first term in (4) can be illustrated as shown in Fig. 1. The primary link PQ has a dual area assigned to it. This area is denoted with the links a, b, c and d. The curl-curl operator is realized as a sum of circulations around all primary surfaces that contain this link. The most-left picture of Fig. 1 illustrates this aspect. The subtraction of the grad-div operator is done in two steps : The grad means that both at P and at Q a divergence is evaluated. The center- and right drawing show these divergences. Next, these terms are added with opposite sign.

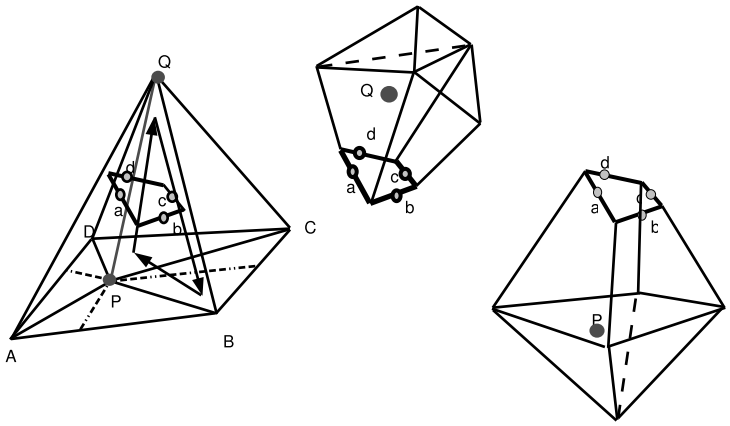

Fig. 1 Discretized version of the regularized curl-curl operator acting on a vector field.

4 The EV Solver

Besides scaling and geometrical considerations, another important ingredient for a successful discretization is to avoid unnecessary matrix fill when selecting dynamical variables. In this section, we present a method to reduce the cross coupling between the V and $\mathbf{A}$ system. Let us consider the Ampere-Maxwell equation. For notational convenience we will introduce the notation: $\phi = \sigma + \mathrm{i}\omega\varepsilon_\mathrm{r}$. Then we can write (7) as

$$\nabla \times \left(\frac{1}{\mu_\mathrm{r}} \nabla \times \mathbf{A} \right) + K\, \phi\, (\nabla V + \mathrm{i}\omega \mathbf{A}) - K\, \mathbf{J}_\mathrm{diff} = 0\,, \tag{9}$$

where $\mathbf{J}_\mathrm{diff}$ is the diffusive part of the current. Furthermore, we will need the gauge condition

$$\nabla \cdot \mathbf{A} + \mathrm{i}\, \omega \xi K\, \varepsilon_\mathrm{r} V = 0\,, \tag{10}$$

where ξ is the slider between 0 (Coulomb gauge) and 1 (Lorentz gauge).
The crucial observation now is that for any scalar field, the equation $\nabla \times \nabla V = 0$ is valid. This leads to

$$\frac{1}{\mathrm{i}\omega}\, \nabla \times \left(\frac{1}{\mu_\mathrm{r}}\, \nabla \times\, [\mathrm{i}\omega\, \mathbf{A} + \nabla V] \right) + K\, \phi\, (\nabla V + \mathrm{i}\omega \mathbf{A}) - K\, \mathbf{J}_\mathrm{diff} = 0\,. \tag{11}$$

We recognize $\mathrm{i}\omega\mathbf{A} + \nabla V = -\mathbf{E}$ and therefore we find that

$$\nabla \times \left(\frac{1}{\mu_\mathrm{r}} \nabla \times \mathbf{E} \right) + K \,\mathrm{i}\, \omega \, \phi \, \mathbf{E} + K \,\mathrm{i}\, \omega \, \mathbf{J}_\mathrm{diff} = 0 \,. \tag{12}$$

Of course, this equation could have been straightforwardly obtained from the Maxwell equations by noting that $\mathbf{B} = -1/(\mathrm{i}\omega)\nabla \times \mathbf{E}$. However, here we consider $\mathbf{E}$ as a variable transformation of $\mathbf{A}$. Just as for the $\mathbf{A}$ system, we must regularize the operator $\nabla \times \nabla \times \mathbf{E}$. This is achieved by subtracting the gauge condition. Using

$$\mathbf{A} = \frac{\mathrm{i}}{\omega} \left(\mathbf{E} + \nabla V \right) \,, \tag{13}$$

we obtain

$$\nabla \cdot \left\{ \frac{\mathrm{i}}{\omega} \left[\mathbf{E} + \nabla V \right] \right\} + \mathrm{i}\, \omega \, K \xi \, \varepsilon_\mathrm{r} \, V = 0 \,. \tag{14}$$

This is equivalent to the following expression :

$$\nabla \cdot \mathbf{E} + \nabla^2 V + \omega^2 K \xi \, \varepsilon_\mathrm{r} \, V = 0 \,. \tag{15}$$

The regularization is now achieved by subtraction of the gradient of equation (15) from equation (12).

$$\begin{aligned} &\nabla \times \left(\frac{1}{\mu_\mathrm{r}} \nabla \times \mathbf{E} \right) - \nabla \left(\nabla \cdot \mathbf{E} \right) + K \,\mathrm{i}\, \omega \, \phi \, \mathbf{E} \\ &- \nabla \left(\nabla^2 V \right) - \omega^2 K \xi \, \nabla \left(\varepsilon_\mathrm{r} V \right) + K \,\mathrm{i}\, \omega \, \mathbf{J}_\mathrm{diff} = 0 \,. \end{aligned} \tag{16}$$

As is seen from this equation the coupling to the variables V has a strength of order one and is not growing with σ. Furthermore it should be noticed that the Poisson equation is not part of the set of equations that must be solved. It is an implicit consequence of the Ampere-Maxwell system. Therefore, the equation to be used for determining V, is the gauge condition :

$$\nabla^2 V + \nabla \cdot \mathbf{E} + K \, \xi \, \omega^2 \, \varepsilon_\mathrm{r} \, V = 0 \,. \tag{17}$$

With equations (16) for the solution of $\mathbf{E}$ and (17) for the solution of V, we can compute the full $\mathbf{E}V$ system. The cross couplings will not explode for large σ in the bulk of the material. Thus we expect that this set-up of equations would have lead to linear systems that will solve faster at high high-frequencies in comparison with the system of equations based on the $\mathbf{A}V$ formulation. However, it should be noted that a third-order derivative term is present. As a consequence the matrix fill increases substantially. We were able to solve (16) and (17) self-consistently for a series of applications at the cost of using *direct* solvers. Finally we note that a full-wave solution needs again *four* fields, i.e. E_x, E_y, E_z and V, to be solved.

4.1 Boundary Conditions

Although no strong coupling exists in the bulk of the material, the boundary conditions introduce again this coupling in some circumstances.
The boundary conditions for the vector equation (16) can be deduced from the boundary conditions for the vector potential **A**. Since for each link in the surface of the simulation domain we have put the boundary condition $\mathbf{A}\cdot\hat{\mathbf{t}}=0$, and $\hat{\mathbf{t}}$ is a tangential unit vector, we obtain

$$\mathbf{E}\cdot\hat{\mathbf{t}}=-\hat{\mathbf{t}}\cdot\nabla V\ . \tag{18}$$

The boundary conditions for the scalar equation (17) can be deduced from the condition that for surface regions outside the contacts, the outward pointing electric field component is taken equal to zero, i.e. $\mathbf{E}\cdot\hat{\mathbf{n}}=0$ where $\hat{\mathbf{n}}$ is a normal unit vector. However, this will not be sufficient to determine the boundary condition for V, since an additional unknown, $\partial V/\partial n$ needs to be given outside the contact regions. Fortunately, there is still room for further restriction. The boundary condition for **A** was only provided for the tangential components of **A**. We will now include also a boundary condition for the normal component of **A** that consists of stating that the normal component of **A** will have be continuous when crossing the simulation surface

$$\hat{\mathbf{n}}\cdot\mathbf{A}_{\text{inside}}=\hat{\mathbf{n}}\cdot\mathbf{A}_{\text{outside}}\ . \tag{19}$$

This can also be written as $\partial A_{\perp}/\partial\, n=0$, or in other words: a Neumann boundary condition is used for the perpendicular component of **A**. However, the surface nodes of the simulation domain can also be determined by applying the Poisson equation and/or current continuity equation for these nodes.

$$\nabla\cdot(\phi\,\mathbf{E}\,)=0\ . \tag{20}$$

For internal nodes, this equation is a consequence of the Maxwell-Ampere system. However, at the surface it must explicitly be enforced by the boundary condition. Thus for the boundary nodes, we apply the Poisson and current-continuity equations, using the inwards pointing link variables E_{ij}. This enables one to get boundary conditions for the V variables on the simulation boundary.

5 Scattering Parameters

In order to determine the S matrix, a rather straightforward procedure is followed. For that purpose a collection of ports is needed and each port consists of two contacts. A contact is defined as a collection of nodes that are electrically identified. A rather evident appearance of a contact is a surface segment on the boundary of the simulation domain. A slightly less trivial contact consists of two or more of

these surfaces on the boundary of the simulation domain. The nodes that are found on these surfaces are all at equal potential. Therefore, although there may be many nodes assigned to a single contact, all these nodes together generate only one potential variable to the system of unknowns. Of course, when evaluating the current entering or leaving the contact, each node in the contact contributes to the total contact current. Assigning prescribed values for the contact potential can be seen as applying Dirichlet's boundary conditions to these contacts. This is a familiar technique in technology CAD. Outside the contact regions, Neumann boundary conditions are applied. Unfortunately, since we are now dealing with the full system of Maxwell equations, providing boundary conditions for the scalar potential will not suffice. We also need to provide boundary conditions for the vector potential. Last but not least, since the set of variable V and $\mathbf{A}$ are not independent, setting a boundary condition for one variable has an impact on the other. Moreover, the choice of the gauge condition also participates in the appearance of the variables and their relations. A convenient set of boundary conditions is given by the following set of rules :

- Contact surface $V = V|_c^i$. To each contact area a prescribed potential value is assigned.
- Outside the contact area on the simulation domain $\mathbf{D}_n = 0$. There is no electric field component in the direction perpendicular to the surface of the simulation domain.
- For the complete surface of the simulation domain, we set $\mathbf{B}_n = 0$. There is no magnetic induction perpendicular to the surface of the simulation domain.

We must next translate these boundary condition to restrictions on $\mathbf{A}$. We start with the last one. Since there is no normal component $\mathbf{B}$, we may assume that the vector potential is perpendicular to the surface of the simulation domain. That means that the links at the surface of the simulation domain do not generate a degree of freedom. It should be noted that more general options exist. Nevertheless, the above set of boundary conditions provide the minimal extension of the TCAD boundary conditions if vector potentials are present.

In order to evaluate the scattering matrix, say of an N-port system, we iterate over all ports and put a voltage difference over one port and put an impedance load over all other ports. Thus the potential variables of the contacts belonging to all but one port, become degrees of freedom that need to be evaluated. The following variables are required to understand the scattering matrices, where Z_0 is a real impedance that is usual taken to be 50 Ohms

$$a_i = \frac{V_i + Z_0 I_i}{2\sqrt{Z_0}} \tag{21}$$

$$b_i = \frac{V_i - Z_0 I_i}{2\sqrt{Z_0}} \,. \tag{22}$$

The variables a_i represent the voltage waves incident on the ports labeled with index i. The variables b_i represent the reflected voltages at ports i. The scattering parameters s_{ij} describe the relationship between the incident and reflected waves

$$b_i = \sum_{j=1}^{N} s_{ij} a_j \ . \tag{23}$$

The scattering matrix element s_{ij} can be found by putting a voltage signal at port i and place an impedance of Z_0 over all other ports. Then a_j is zero by construction, since for those ports we have that $V_j = -Z_0 I_j$. Note that I_j is defined positive if the current is ingoing. In this configuration $s_{ij} = b_i/a_j$. In a simulation setup, we may put the input signal directly over the contacts that correspond to the input port. This would imply that the input load is equal to zero. The *s*-parameter evaluation set up is illustrated in Fig. 2.

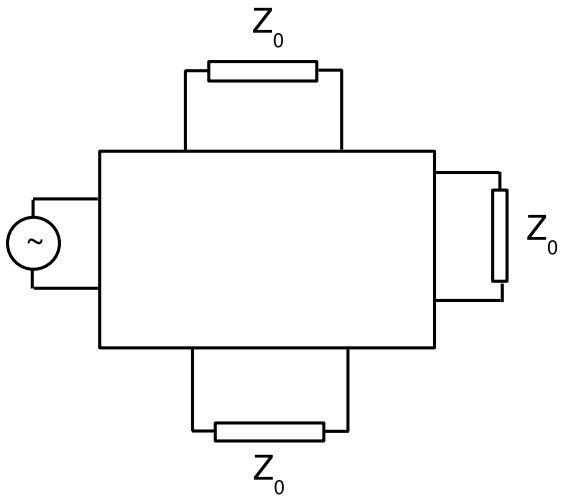

Fig. 2 Set up of the *s*-parameter evaluation: 1 port is excited and all others are floating.

6 Applications

Using the solver based on computational electrodynamics, we are able to compute the s-parameters by setting up a field simulation of the full structure. This allows us to study in detail the physical coupling mechanisms. As an illustration, we consider two inductors which are positioned on a substrate layer separated by a distance of 14 micron. This structure was processed and characterized and the *s*-parameters were obtained. It is quite convenient when studying a compact model parameters to obtain a quick picture of the behavior of the structure. For this device a convenient variable is the 'gain', which corresponds to the ratio of the injected power and the delivered power over an output impedance [11]

$$G = \frac{P_{in}}{P_{out}} \, . \tag{24}$$

The structure is shown in Fig. 3.

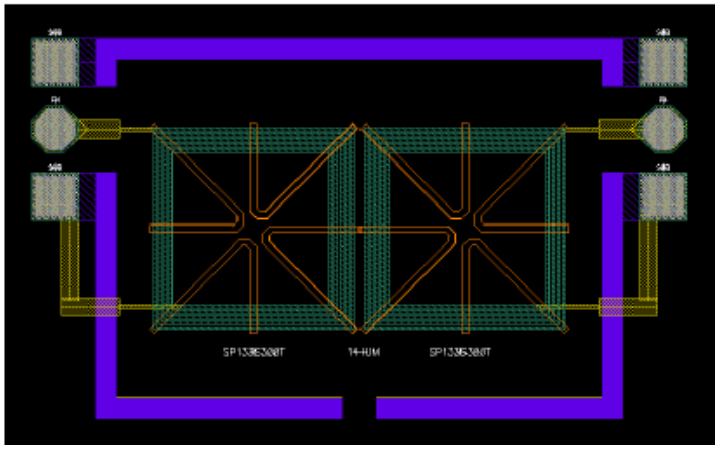

Fig. 3 View on the coupled spiral inductor using the Virtuosa design environment.

When computing the *s*-parameters, we put the signal source on one spiral (port 1) and place 50 Ohm impedance over the contacts of the second spiral (port 2).The s_{11}-parameter is shown in Fig. 4 and the s_{12}-parameter is shown in Fig. 5. Finally,

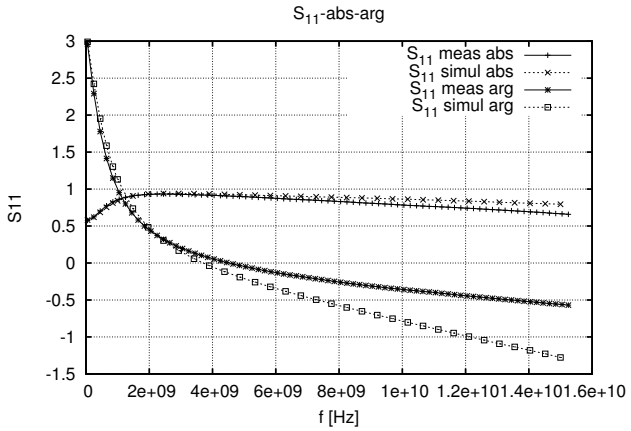

Fig. 4 Comparison of the experiment and simulation results for s_{11} .

the gain plot is shown in Fig. 6. This results shown here have been obtained without any calibration of the material parameters. The silicon is treated 'as-is'. This means

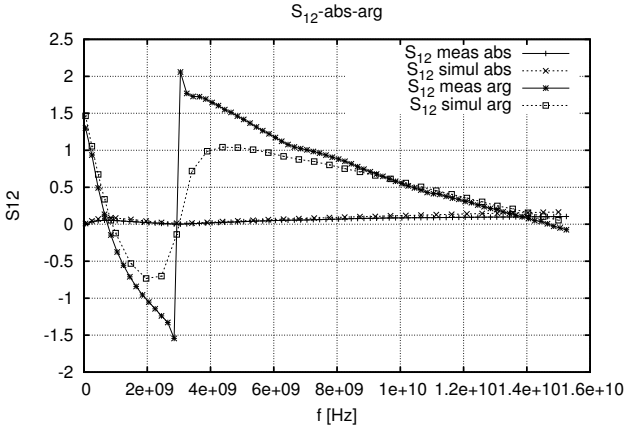

Fig. 5 Comparison of the experiment and simulation results for s_{12} .

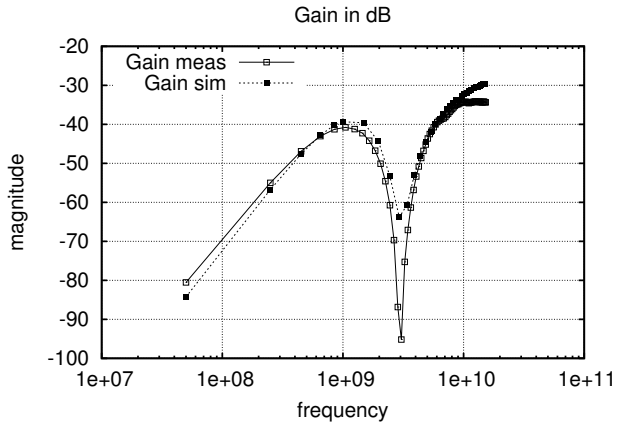

Fig. 6 Comparison of the experimental and simulation results for the gain.

that the substrate and the eddy current suppressing n-wells are dealt with as doped silicon.

7 Conclusions

In this paper we presented a version of computational electrodynamics which is based on the scalar and vector potential formulation. Whereas the finite-integration technique directly deals with the field intensity quantities **E** and **B**, our formulation deals with the more fundamental gauge fields. It should be emphasized that the field quantities are derived variables and once that the potentials have been computed,

whereas all other variables are obtained by 'post-processing'. Our approach is a discrete implementation of the geometrical interpretation of electrodynamics [12]. According to this interpretation, the field intensities correspond to the curvature and the potentials are connections in the geometrical sense. The practical capabilities of our method are comparable to other field solvers that focus directly on the fields **E** and **B**, with one exception: if the potentials are needed in the evaluation of the constitutive relations then our method has a clear advantage. This happens if semiconductor modeling is needed and one can not mimic the semiconductor with moderately conductive material. Another area of application is the unified solving of quantum problems and magnetic induction problems where the potential approach is definitely the most natural choice. We have shown with a realistic application that the method is capable of producing fairly good results. The deviations at higher frequency are an indication that adaptive meshing methods are mandatory.

Acknowledgements This work was performed in the EU funded projects CODESTAR (IST-2001-34058) CHAMELEON-RF (FP6-2004-IST-4-027378) ICESTARS (FP7-214911) and the IP project PULLNANO (IST 026828). The authors acknowledge the numerous stimulating discussions with the partners in this project.

References

1. Meuris, P., Schoenmaker, W., W, M.: Strategy in Electromagnetic Interconnect Modeling. IEEE Trans. on CAD of Integr. Syst. **20**, 739–752 (2001)
2. Schoenmaker, W., Meuris, P.: Electromagnetic interconnects and passives modeling: Software implementation issues software implementation issues. IEEE Trans. on CAD of Integr. Syst. **21**, 534–543 (2002)
3. Schoenmaker, W., Magnus, W., Meuris, P.: Ghost fields in classical gauge theories. Phys. Rev. Lett. **88**, 181,602–1 – 181,602–4 (2002)
4. Nedelec, J.C.: Mixed finite elements in r^3. Numer. Math. **35**, 315–341 (1980)
5. Lee, J.F.S.D.K., J, C.Z.: Tangential vector finite elements for electromagnetic field computation. IEEE Transactions on Magnetics **27**, 4032–4035 (1991)
6. Weiland, T.: A discretization method for the solution of maxwells equations for six-component fieldss. Electronics and Communications AEU **31 No. 3**, 116120 (1977)
7. Schuhmann, R., Weiland, T.: A stable interpolation technique for fdtd on nonorthogonal grids. International Journal on Numerical Modelling **11**, 299306 (May 1998)
8. Bossavit, A.: Discretization of electromagnetic problems: The "generalized finite differences" approach. In: W.H.A. Schilders, E.J.W. ter Maten (Eds), Handbook of numerical analysis , Elsevier North-Holland **XIII**, 105–197 (2005)
9. Bossavit, A.: The sommerville mesh in yee-like schemes. In: W.H.A. Schilders, E.J.W. ter Maten, S.H.M.J. Houben, Scientific computing in electrical engineering, Series Maths. Series Mathematics in Industry , Springer **4**, 128–136 (2003)
10. Scharfetter, D., Gummel, H.: Large signal analysis of a silicon read diode oscillator. IEEE Trans. Electron Devices **ED-16**, 66–77 (1969)
11. Niknejad, A.M., Meyer, R.G.: Analysis, design and optimization of spiral inductors and transformers for si rf ics. IEEE Journ. of Solid-State Circuits **33**, 1470–1481 (1998)
12. Frankel, T.: The Geometry of Physics. University Press, Cambridge (1997)